Sustainable Energy & Fuels

Improved water oxidation under visible light on oxyhalide Bi_4MO_8X (M = Nb, Ta; X = Cl, Br) photocatalysts prepared using excess halogen precursors

Journal:	*Sustainable Energy & Fuels*
Manuscript ID	SE-ART-02-2018-000097.R2
Article Type:	Paper
Date Submitted by the Author:	27-Mar-2018

Complete List of Authors:	Kunioku, Hironobu; Kyoto University, Graduate School of Engineeing Nakada, Akinobu; Kyoto University Higashi, Masanobu; Kyoto University, Tomita, Osamu; Kyoto University, Energy and Hydrocarbon Chemistry Kageyama, Hiroshi; Kyoto University, Department of Energy and Hydrocarbon Chemistry Abe, Ryu; Kyoto University, Graduate School of Engineeing

Journal Name

ARTICLE

Improved water oxidation under visible light on oxyhalide Bi_4MO_8X (M = Nb, Ta; X = Cl, Br) photocatalysts prepared using excess halogen precursors

Received 00th January 20xx,
Accepted 00th January 20xx

DOI: 10.1039/x0xx00000x

www.rsc.org/

Hironobu Kunioku,[a] Akinobu Nakada,[a] Masanobu Higashi,[a] Osamu Tomita,[a] Hiroshi Kageyama[a,b,*] and Ryu Abe[a,b,*]

We herein report the synthesis of a series of Bi-based oxyhalides Bi_4MO_8X (M = Nb, Ta; X = Cl, Br) *via* solid-state reaction at different calcination temperatures and using various precursor ratios to improve their photocatalytic activity for water oxidation under visible light. The calcination temperature employed gave an influence on the crystallite sizes, morphologies, specific surface areas, and surface compositions. Interestingly, when stoichiometric precursors were heated at higher temperatures, the crystallite sizes of Bi_4MO_8X decreased with cleavage occurring along in-plane direction. Elemental analysis indicated that the unusual trend in Bi_4MO_8X can be explained by the volatile nature of halogen at higher temperatures. The volatilization of the halogen species was minimized when an excess of the halogen precursor BiOX was employed. The Bi_4MO_8X samples prepared with excess BiOX exhibited considerably higher photocatalytic activities for water oxidation under visible light, due to the suppressed halogen defects at which recombination of photogenerated carriers can occur. These findings offer a useful insight into the preparation of active oxyhalide photocatalysts.

Introduction

Visible-light-induced water splitting using semiconductor photocatalysts has attracted significant attention due to the potential for clean hydrogen (H_2) production using abundant solar light.[1-3] Over the past decade, various mixed-anion compounds such as oxynitrides,[4-7] oxysulfides,[8] and oxyhalides[9] have been studied extensively as promising photocatalyst materials for visible-light-induced water splitting since one can expect that higher energy p-orbitals of non-oxide anions (*e.g.*, N-2p, S-3p, Br-4p, and I-5p) elevate their valence band maximum (VBM) values and consequently decrease the bandgaps.[10] However, the majority of these compounds suffer from self-oxidative deactivation during water oxidation, in which the photogenerated holes oxidize the non-oxide anions themselves (*e.g.*, $2N^{3-} + 6h^+ \rightarrow N_2$) instead of water molecules.[11] A number of efforts have been made to circumvent such oxidative deactivation, but they mostly concern surface modifications such as loading some cocatalysts.[12, 13]

Very recently, we have demonstrated that a series of oxyhalides Bi_4MO_8X (Fig. 1, M = Nb, Ta; X = Cl, Br) with a Sillén-Aurivillius perovskite phase can function as stable O_2-evolving photocatalysts under visible-light irradiation.[14, 15] It was revealed that the VBMs in Bi_4MO_8X consist mainly of O-2p orbitals, instead of Cl-3p or Br-4p, while their levels are located at much more negative than those of usual oxides or oxychlorides.[14] DFT calculations have visualized a fairly strong hybridization between the Bi-6s orbitals and the O-2p orbitals, which explain why the O-2p orbitals are elevated in energy.[15] A Madelung site potential analysis further revealed that the upward shift of the valence band lies in the oxygen site in the fluorite-based $[Bi_2O_2]$ layer.[16] Since O^{2-} anions are relatively stable, photogenerated holes populated at the O-2p orbitals will not lead to self-decomposition but to the oxidation of water.

It is well recognized that the rational design of photocatalyst surfaces, in addition to the tuning of bulk properties such as bandgaps, is of particular importance for achieving optimal photocatalyst activities.[17-23] For example, the activity of perovskite-type oxides photocatalysts, *i.e.*, $MTaO_3$ (M = Li, Na, or K), for overall water splitting (*i.e.*, simultaneous generation of H_2 and O_2) under UV light is greatly enhanced by the addition of excess (5–10%) alkaline precursor in the solid-state reaction at high temperatures, as this addition effectively produces a favorable surface morphology of particles for the efficient charge separation and water oxidation.[24] However, such attempts on oxyhalides particles have been limited. While some oxyhalides (*e.g.*, BiOX) are prepared *via* soft-chemical methods in solution, the preparation of Bi_4MO_8X requires high temperature solid state reaction. In our previous study, Bi_4MO_8X particles were

[a] Department of Energy and Hydrocarbon Chemistry, Graduate School of Engineering, Kyoto University, Nishikyo-ku, Kyoto 615-8510, Japan. E-mail: kage@scl.kyoto-u.ac.jp (H.K.); ryu-abe@scl.kyoto-u.ac.jp (R.A.)
[b] CREST, Japan Science and Technology Agency (JST), Kawaguchi, Saitama 332-0012, Japan.

Electronic Supplementary Information (ESI) available: Lattice constant, XRD patterns, SEM images, Atomic composition and photocatalytic activities. See DOI: 10.1039/x0xx00000x

obtained by heating of a stoichiometric mixture of precursors in a sealed quartz tube under vacuum at 1073 K. Neither detailed surface analysis nor morphology optimization for improving activity were examined.

Here we report the preparation of Bi_4MO_8X (M = Nb, Ta; X = Cl, Br) under a range of calcination temperatures and precursor ratios to understand the influence of the physicochemical properties such as surface morphology and composition on the photocatalytic activity. The aim of this study is to gain insight into the strategy for improving the activity of oxyhalide photocatalysts in general.

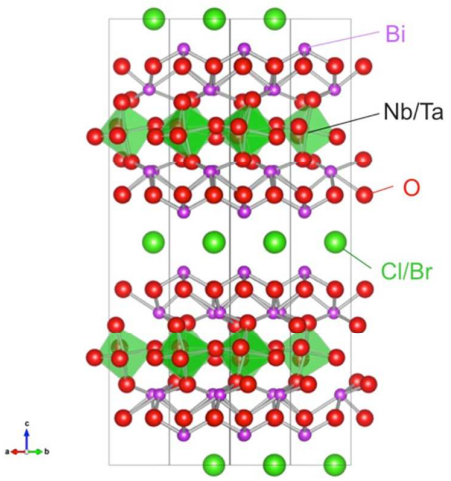

Fig. 1 Crystal structure of Bi_4MO_8X (M = Nb, Ta; X = Cl, Br).

Experimental

Sample synthesis

Particulate samples of Bi_4MO_8X (M = Nb, Ta; X = Cl, Br) were prepared *via* solid state reactions,[25, 26] with stoichiometric precursors (denoted as BMOX) or with addition of an excess of the halogen precursor (denoted as ex-BMOX). For the preparation of Bi_4NbO_8Cl and Bi_4TaO_8Cl with stoichiometric precursors (denoted as BNOC and BTOC, respectively), a stoichiometric mixture of Bi_2O_3 (Wako Pure Chemical Industries, Ltd., 99.99%), BiOCl (Wako Pure Chemical Industries, Ltd., 99.9%), and Nb_2O_5 (Wako Pure Chemical Industries, Ltd., 99.9%) for BNOC or Ta_2O_5 (Wako Pure Chemical Industries, Ltd., 99.9%) for BTOC was pelletized and evacuated in a quartz tube. The quartz tube was sealed by high-temperature flame and then heated in an electrical furnace at a set temperature between 973 and 1173 K for 20 h. For the preparation of samples with an excess amount of a chloride precursor, 5, 10 or 15 mol% excess of BiOCl was added to the stoichiometric mixture, and the resulting mixture was pelletized and heated in a similar manner. The obtained samples from 5 mol% excess BiOCl will be denoted as ex-BNOC and ex-BTOC. The Bi_4NbO_8Br and Bi_4TaO_8Br samples were synthesized in a similar manner but by using home-made BiOBr particles prepared *via* a soft liquid deposition method as described elsewhere.[24] $Bi(NO_3)_3{\cdot}5H_2O$ (5 mmol, Wako Pure Chemical Industries, Ltd., 99.9%) was dissolved in ethanol (30 mL), and a solution of KBr (5 mmol, Wako Pure Chemical Industries, Ltd., 99.9%) dissolved in Milli-Q water (10 mL) was added to the above solution. The resulting solution was then stirred for 5 h at 298 K to give a precipitate, which was subsequently filtered, washed with water several times, and dried at 353 K for 5 h. The Bi_4NbO_8Br and Bi_4TaO_8Br samples prepared using a stoichiometric ratio will be denoted by BNOB and BTOB, respectively, while those prepared using 5 mol% excess of BiOBr will be denoted by ex-BNOB and ex-BTOB, respectively. For comparison, some samples were prepared by adding 5% excess of KCl, KBr or Bi_2O_3 in place of BiOCl or BiOBr.

Characterization

The prepared samples were characterized by powder X-ray diffraction (XRD; MiniFlex II, Rigaku, Cu Kα), scanning electron microscopy (SEM; NVision 40, Carl Zeiss-SIINT), UV-visible diffuse reflectance spectroscopy (V-650, Jasco), energy-dispersive X-ray spectroscopy (EDX; X-max, Oxford Instruments), and X-ray photoelectron spectroscopy (XPS; ESCA5500, ULVAC-PHI; Mg Kα). The XPS binding energies for each sample were corrected with reference to the C 1s peak of the carbon impurity (284.8 eV). Angle-resolved XPS (ARXPS) measurements were performed by controlling the take-off angle, which is defined as the angle between the plane of the surface and the analyzer axis. The lattice parameters were determined by Le Bail analysis using the Jana2006 program.[27] The specific surface areas of samples were determined by Brunauer-Emmett-Teller (BET) measurements (BELSORP-mini II, MicrotracBEL Corp.) at liquid nitrogen temperature.

Photocatalytic reactions

Photocatalytic O_2 evolution was carried out using a Pyrex glass reactor. A portion of the photocatalyst powder (0.1 g) was suspended in a solution of $AgNO_3$ (123 mL, 5 mM, without pH adjustment). Prior to starting photocatalytic reaction, the suspension was purged with Ar gas for more than 30 min to remove the dissolved air. Then, the suspension was irradiated using a 300 W Xe lamp fitted with a cut-off filter (λ > 400 nm). The evolved O_2 gas was detected by means of an on-line gas chromatograph (Agilent MicroGC 3000A) equipped with a thermal conductivity detector (TCD) and an MS-5A column. Ar was employed as the carrier gas.

Results and discussion

Influence of calcination temperature on Bi_4MO_8X particles

Figs. 2 and 3 show the XRD patterns of BMOX and ex-BMOX samples prepared at various temperatures. The solid-state reaction at 973–1173 K yielded an almost pure orthorhombic phase of Bi_4MO_8X with a space group of *P*21*cn*,[25, 26] while lower temperature reactions provided small unassignable peaks. In addition, no variation in lattice constants owing to changing calcination temperature was observed for BMOX samples (Fig. S1). As shown in Fig. 2a, upon increasing the

calcination temperature to obtain BNOC, the intensity of the XRD peak corresponding to the (00*l*) reflection increased, indicating that BNOC adopts the preferred *c*-axis orientation following calcination at high temperatures. The ex-BMOX samples were also obtained as pure phases when reacted at 1073 and 1173 K (Figs. 2 and 3). Although excess BiOX (X = Cl, Br) was employed as the halogen precursor, no XRD peaks for BiOX were observed in ex-BMOX (*i.e.*, the powder samples obtained by the pulverization of pellet). As shown in Fig. S2, white BiOX crystals were adhered on the inner wall of the quartz-tube, along with a small amount of yellow Bi_4MO_8X particles.

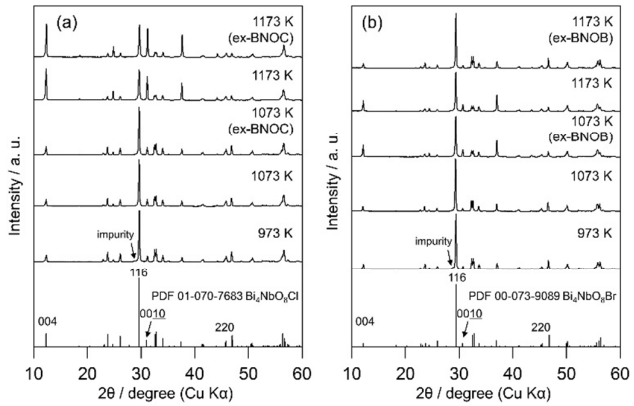

Fig. 2 XRD patterns of the (a) BNOC and ex-BNOC, and (b) BNOB and ex-BNOB samples calcined between 973 and 1173 K.

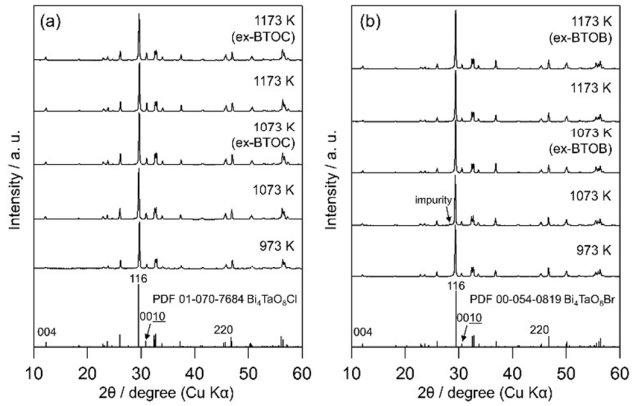

Fig. 3 XRD patterns of the (a) BTOC and ex-BTOC, and (b) BTOB and ex-BTOB samples calcined between 973 and 1173 K.

Fig. 4 summarizes the estimated crystallite sizes for layer (*c*-axis) and in-plane (*ab*-axis) directions, which were estimated on the basis of the Scherrer equation using diffraction peaks attributable to (00$\underline{1}$0) and (220), respectively (Eq. 1).

$$\tau = \frac{K\lambda}{\beta \cos\theta} \qquad (1)$$

where τ, K, λ, β and θ indicate crystallite size (nm), shape factor (0.94 assumed to be cubic particles), X-ray wavelength (nm), full width at half maximum (rad) and Bragg angle (degree), respectively. The estimated crystallite sizes of both BNOX and BTOX samples for the layer direction increased upon increasing the calcination temperature up to 1173 K. The estimated crystallite sizes for the in-plane direction also increased with increasing temperature up to 1073 and 1123 K for BNOX and BTOX, respectively. However, they decreased obviously at higher temperatures. Note that such decrease in the crystal size for in-plane direction at higher temperatures was much more noticeable for niobium compounds BNOX than for tantalum ones BTOX. The reduction in crystallite size upon increasing calcination temperature is unprecedented. In metal oxides such as $SrTiO_3$ and WO_3,[17, 28] the crystallite sizes basically increase with increasing calcination temperature due to crystal growth. The decreased crystallite sizes for the in-plane direction estimated from (220) peaks, especially for BNOX samples at above 1073 K, suggest the cleavage along in-plane direction at high temperatures.

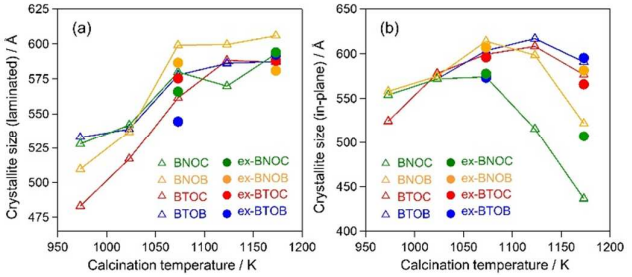

Fig. 4 Crystallite sizes for (a) layer and (b) in-plane directions estimated using the (00$\underline{1}$0) and (220) peaks in the XRD patterns of the BMOX and ex-BMOX samples calcined between 973 and 1173 K.

As seen in Fig. 5, the particle size of the dominant BNOC particles was obviously increased from several hundred nanometers to 1~ 2 μm with increasing temperature from 973 to 1073 K, however, a number of small and plate-like particles emerged after calcination at 1073 K. The fraction of such small particles considerably increased in the sample prepared at 1173 K, along with the appreciable reduction in size of dominant BNOC particles. The same tendency was observed for BNOB samples (Fig. S3). Although such small particles at high temperatures were observed also for BTOX (see Figs. S4 and S5), the effect was less prominent compared to BNOX (see Fig. 5). The change in the BET specific surface areas (Table 1) also supports the destruction of particles at high temperatures. This phenomenon is not so simple because both growth and destruction of crystal should simultaneously proceed. Until 1073 K, the specific surface areas of BNOX slightly reduced and then drastically increased at higher temperatures. On the other hand, such effect was much less prominent in BTOX (Table 1). Note that the crystal growth along the *c* axis proceeds on both BNOX and BTOX particles as the temperature increased, as seen in Fig. 4a where the crystalline sizes for the layer direction increased with increasing calcination temperature.

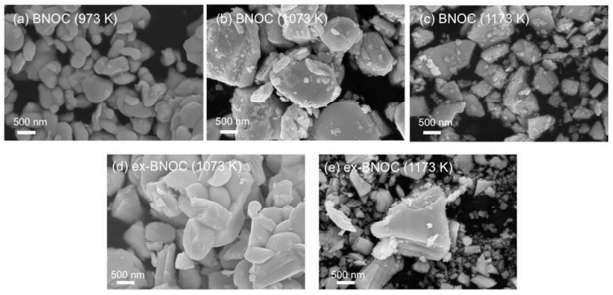

Fig. 5 SEM images of the BNOC samples calcined at (a) 973 K, (b) 1073 K, and (c) 1173 K, and the ex-BNOC samples calcined at (d) 1073 K and (e) 1173 K.

Effect of addition of excess halogen precursor BiOX

As described above, the elevated calcination temperature of stoichiometric precursors (at above 1073 K) resulted in the reduced crystalline size of BMOX samples, specifically in BNOX ones. The observed trend is unusual since in general higher temperature calcination increases the crystalline size. Such trend on BMOX may be explained by the volatile nature of halogen at high temperatures. This speculation led us to employ an excess of the halogen precursor, BiOX, and we found that this effectively suppresses the cleavage of BNOX crystals during calcination at high temperatures, at least to some extent. As seen in Fig. 4b, the crystalline sizes for the in-plane direction of ex-BNOX prepared at 1173 K are considerably larger than those of BNOX. Although the crystalline sizes for the in-plane direction of ex-BNOX estimated by the Scherrer equation are comparable to those of BNOX at 1073 K (Fig. 4b), SEM images indicated that the addition of excess BiOX effectively suppress the generation of small particles. As for BTOX, the addition of BiOX provides a limited influence on the estimated crystalline sizes for the in-plane direction up to 1173 K, however, it actually suppresses the formation of small particles as clearly confirmed by their SEM images. This is supported by BET surface areas of ex-BMOX compared to the stoichiometric BMOX (Table 1 and 2). Thus, it can be concluded that the addition of excess BiOX precursor can effectively suppress the cleavage of crystals during calcination at high temperatures. As described in the previous section, no peaks corresponding to BiOX were observed in the XRD patterns of main products of ex-BMOX, due to the volatile nature of BiOX, as seen on the inner wall of the quartz-tube (Fig. S2).

Table 1 BET specific surface areas of the Bi_4MO_8X samples calcined between 973 and 1173 K

Temperature	BET specific surface area / $m^2\ g^{-1}$			
	BNOC	BNOB	BTOC	BTOB
973 K	1.2	1.1	1.0	0.9
1023 K	1.2	1.1	1.1	0.9
1073 K	1.4	0.6	0.9	0.9
1123 K	1.8	1.2	0.8	1.1
1173 K	2.7	2.6	0.9	1.5

Table 2 BET specific surface areas of the ex-BMOX samples calcined at 1073 and 1173 K

Temperature	BET specific surface area / $m^2\ g^{-1}$			
	ex-BNOC	ex-BNOB	ex-BTOC	ex-BTOB
1073 K	1.1	0.8	1.1	1.0
1173 K	2.4	2.0	0.7	1.4

Fig. 6 shows the UV-vis diffuse reflectance spectra of the BMOX and ex-BMOX samples calcined at 1073 K, where the absorption edges of the BMOX spectra shifted towards longer wavelength in the order BTOB (~470 nm) < BTOC (~480 nm) < BNOB (~485 nm) < BNOC (~495 nm). These results were in good agreement with our previous report.[15] The absorption edges of the ex-BMOX samples were similar to the corresponding BMOX samples, indicating that the addition of excess BiOX precursor does not interfere with the absorption properties of these materials.

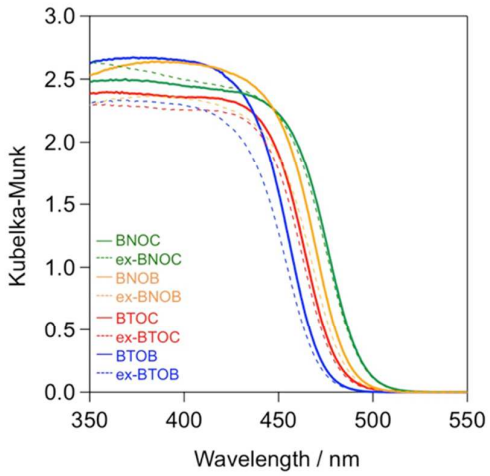

Fig. 6 UV-vis diffuse reflectance spectra of the BMOX and ex-BMOX samples calcined at 1073 K.

Tables 3 and 4 summarize the element ratios of halogen/bismuth (X/Bi) in the BMOX and ex-BMOX samples, respectively, as determined by XPS. As seen in Table 3, the X/Bi ratios of all BMOX samples decreased upon increasing the calcination temperature, due to volatilization of the halogen

species. These results strongly suggest that the aforementioned changes in morphology and particle size upon increasing the calcination temperature were basically triggered by a release of halogen species. In contrast, the ex-BMOX samples exhibited slightly but appreciably higher X/Bi ratios compared to those of the BMOX samples, strongly suggesting that the excess use of BiOX compensates the halogen volatilization. On the other hand, the Ta/Bi ratios were almost identical (*e.g.* Ta/Bi = 0.25 in BTOC samples synthesized at 1073 K with and without excess BiOCl). Although XPS analysis is basically sensitive to the elements that exist at the surface of specimen due to the short escape depth of photoelectrons, the obtained results often include the information of bulks near surface to some extent. We carried out an angle-resolved XPS (ARXPS) measurement to determine the X/Bi ratios near the surface accurately and to evaluate the effect of BiOX addition on the surface composition (*i.e.*, X/Bi ratios). In ARXPS measurement, the information near surface can be obtained more selectively by decreasing the take-off angle, which is defined as the angle between the plane of the surface and the analyzer axis. Since the ex-BTOC showed drastically improved activity compared to BTOC as will be shown and discussed in the next section, we selected the BTOC and ex-BTOC samples prepared at 1073 K, which respectively exhibited Cl/Bi ratios of 0.24 and 0.25 *via* normal XPS analysis, for further analysis by ARXPS. As shown in the ARXPS measurements presented in Fig. 7, the Cl/Bi atomic ratio in BTOC decreased significantly upon decreasing the take-off angle. In contrast, only a small decrease in the Cl/Bi ratio was observed in the ex-BTOC sample, suggesting that the surface defects caused by the halogen species were indeed suppressed. These results therefore indicate that volatilization of the halogen species was minimized when an excess of the halogen precursor (*i.e.*, BiOX) was employed during solid-state reaction.

Table 3 Halogen/bismuth (Cl/Bi or Br/Bi) atomic ratios in the BMOX samples calcined between 973 and 1173 K, as determined by XPS

Temperature	Cl/Bi or Br/Bi			
	BNOC	BNOB	BTOC	BTOB
973 K	0.31	0.27	0.27	0.27
1023 K	0.31	0.27	0.25	0.26
1073 K	0.26	0.25	0.24	0.24
1123 K	0.25	0.24	0.24	0.25
1173 K	0.24	0.22	0.20	0.23

Table 4 Halogen/bismuth (Cl/Bi or Br/Bi) atomic ratios in the ex-BMOX samples calcined at 1073 and 1173 K

Temperature	Cl/Bi or Br/Bi			
	ex-BNOC	ex-BNOB	ex-BTOC	ex-BTOB
1073 K	0.29	0.26	0.25	0.26
1173 K	0.27	0.23	0.25	0.24

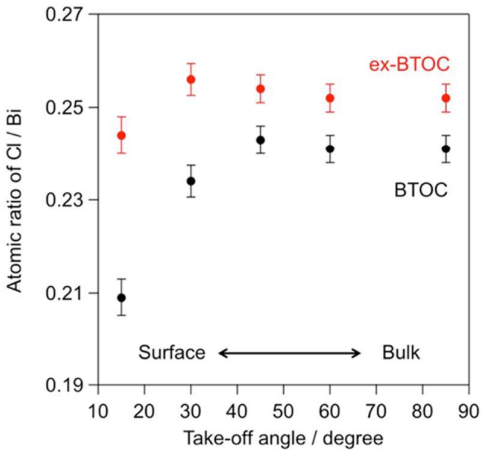

Fig. 7 Cl/Bi atomic ratios for the BTOC and ex-BTOC samples determined by angle-resolved XPS (ARXPS) measurements.

Photocatalytic activity of Bi_4MO_8X samples for water oxidation under visible light irradiation

Fig. 8 shows the initial rate of O_2 evolution on BMOX and ex-BMOX in a 5 mM aqueous $AgNO_3$ solution under visible light irradiation (λ > 400 nm). As for the BMOX samples prepared from stoichiometric precursors, the rates of O_2 evolution increased with increasing calcination temperature from 973 to 1073 K, likely due to enhanced crystal growth (see Fig. 4). However, upon increasing the calcination temperature above 1073 K, the O_2 evolution rate decreased to a lesser or greater degree; the decrease is more prominent in chloride-contained samples (BNOC and BTOC). The lowered activity at higher temperatures is likely due to the formation of crystal defects attributed to volatilization of the halogen species and/or cleavage of crystals. Such crystal defects have been reported to trap photoexcited electrons and accelerate the recombination between the electrons and holes, occasionally lowering the photocatalytic activity.[29, 30] Thus, the significant enhancement of photocatalytic activity occurred with a decrease of anion defects of the present BMOX samples, although opposite phenomena, *i.e.*, defects accelerate photocatalytic reaction, also happen.[31, 32]

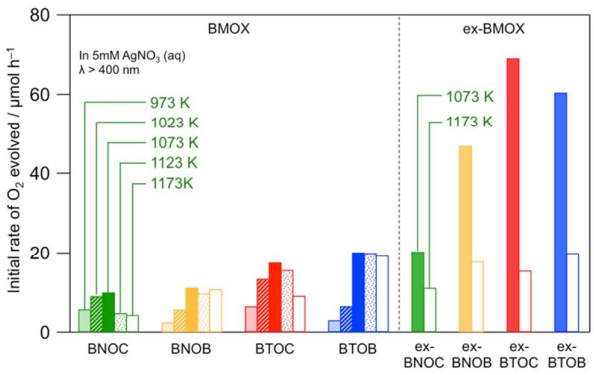

Fig. 8 Initial rates of O_2 evolution over various BMOX and ex-BMOX samples in an aqueous $AgNO_3$ solution (5 mM) under visible light irradiation ($\lambda > 400$ nm).

Importantly, all ex-BMOX photocatalysts, which were prepared with 5 mol% excess of BiOX, exhibited higher rates of O_2 evolution than the corresponding BMOX samples when compared at each temperature (1073 or 1173 K). More specifically, the ex-BTOC sample calcined at 1073 K exhibited the highest activity, with an apparent quantum yield (AQY) for O_2 evolution being ~2.3% at 420 nm in an aqueous $AgNO_3$ solution. This value was substantially higher than that of BTOC (~0.8%) under the same reaction conditions. It was therefore assumed that the generation of halogen (and/or oxygen to some extent) defects was suppressed through the use of excess BiOX during preparation, thus enhancing the photocatalytic activity. O_2 generation continuously proceeded as seen in an example of ex-BTOC (Fig. S6). Although we note that the rate of O_2 formation gradually decreased, this is likely due to light shading by Ag deposited via oxidation of Ag^+ as previously reported.[14] It was difficult to obtain reliable XPS data to estimate a Cl/Bi ratio after photocatalytic reaction with Ag^+ electron acceptor because Ag metal species coated the surface of BMOX. However, we previously investigated the photostability of BMOX using an photoelectrochemical method in Na_2SO_4 solution, where the Cl/Bi ratio almost unchanged.[15] To gain further insight into the effect of an excess of the halogen precursor, the excess quantity of BiOCl was varied between 0 and 15 mol%, and the corresponding photocatalytic activities were measured, paying particular attention to the effect on the ex-BTOC sample calcined at 1073 K. Although the rates of O_2 evolution increased upon increasing the excess halogen quantity from 0 to 5 mol%, the rate decreased slightly with a further increase from 5 to 15 mol% (Table S1). In addition, analysis by XPS and EDX indicated almost no change in the Cl/Bi atomic ratio at excess quantities >5 mol% (Table S1). Furthermore, other ex-BTOC samples were also synthesized using excess KCl to evaluate the effects of an alternative halogen precursor. As shown in Fig. S7, BTOC prepared in the presence of excess KCl exhibited a higher rate of O_2 evolution (26 μmol h^{-1}) than the BTOC sample prepared using a stoichiometric halogen ratio (18 μmol h^{-1}), although this rate was significantly lower than that of the BTOC sample prepared in the presence of excess BiOCl (69 μmol h^{-1}). A similar trend was also observed for the BTOB sample prepared in the presence of excess KBr. On the other hand, the additional Bi_2O_3 precursor in the synthesis of BTOX samples did not increase O_2 evolution rate, strongly suggesting that the excess amount of Bi in samples is not the main reason for the improved photocatalytic activity by using the excess BiOX precursors. We can therefore conclude that the addition of excess halogen species during preparation enhanced the photocatalytic activity of these materials regardless of halogen precursor, while the addition of BiOX is most effective at present. Another important finding is that BTOX generally exhibited a higher photocatalytic activity than BNOX at any calcination temperatures independent of the use of excess halogen precursor, in spite of shorter absorption edges of BTOX compared to BNOX, implying that BTOX possess greater potential as an efficient O_2-evolving photocatalyst.

Conclusions

We reported the synthesis of a series of Bi-based oxyhalides (*i.e.*, Bi_4MO_8X; M = Nb, Ta; X = Cl, Br) under a range of calcination temperatures and precursor ratios to examine the effect of these variables on the activity of oxyhalide photocatalysts for water oxidation under visible light. Following evaluation of the crystallite sizes, morphologies, specific surface areas, and surface compositions of the products, it was revealed that the photocatalytic activities of the various Bi_4MO_8X samples were significantly affected by calcination temperature, likely due to the volatilization of halogen species present in these materials at high temperatures. Such volatilization results in the formation of defects on the surface and in the bulk, which can act as recombination centers of photogenerated carriers and consequently reduce the rate of O_2 evolution. Thus, we found that ex-BMOX samples prepared using an excess of the halogen precursors exhibited superior photocatalytic activities for the oxidation of water under visible light compared to the BMOX samples prepared using a stoichiometric ratio of precursors. Furthermore, the use of a suitable halogen precursor was essential to suppress the formation of halogen defects during calcination. The findings shown in the present study will be expected to offer a useful insight into the preparation of active oxyhalide photocatalysts.

Conflicts of interest

There are no conflicts to declare.

Acknowledgements

This work was supported by the CREST (JPMJCR1421) and JSPS KAKENHI (JP17H06439, JP16H06439, JP16H06441, and JP15H03849). The authors are also indebted to the technical division of Institute for Catalysis, Hokkaido University for their help in building the experimental equipment. H.K. The work was partly supported by Japan Society for the Promotion of

Science (JSPS) Core-to-Core Program (A) Advanced Research Networks.

Notes and references

1. F. E. Osterloh, *Chem. Mater.*, 2008, **20**, 35-54.
2. R. Abe, *J. Photochem. Photobiol. C: Photochem. Rev.*, 2010, **11**, 179-209.
3. A. Kudo and Y. Miseki, *Chem. Soc. Rev.*, 2009, **38**, 253-278.
4. K. Maeda, K. Teramura, D. Lu, T. Takata, N. Saito, Y. Inoue and K. Domen, *Nature*, 2006, **440**, 295-295.
5. Y. Lee, H. Terashima, Y. Shimodaira, K. Teramura, M. Hara, H. Kobayashi, K. Domen and M. Yashima, *J. Phys. Chem. C*, 2007, **111**, 1042-1048.
6. C. Pan, T. Takata, M. Nakabayashi, T. Matsumoto, N. Shibata, Y. Ikuhara and K. Domen, *Angew. Chem. Int. Ed.*, 2015, **54**, 2955-2959.
7. J. Xu, C. Pan, T. Takata and K. Domen, *Chem. Commun.*, 2015, **51**, 7191-7194.
8. A. Ishikawa, T. Takata, J. N. Kondo, M. Hara, H. Kobayashi and K. Domen, *J. Am. Chem. Soc.*, 2002, **124**, 13547-13553.
9. J. Li, Y. Yu and L. Zhang, *Nanoscale*, 2014, **6**, 8473.
10. H. Kageyama, K. Hayashi, K. Maeda, J. P. Attfield, Z. Hiroi, J. M. Rondinelli and K. R. Poeppelmeier, *Nat. Commun.*, 2018, **9**, 772.
11. A. Kasahara, K. Nukumizu, G. Hitoki, T. Takata, J. N. Kondo, M. Hara, H. Kobayashi and K. Domen, *J. Phys. Chem. A*, 2002, **106**, 6750-6753.
12. R. Abe, M. Higashi and K. Domen, *J. Am. Chem. Soc.*, 2010, **132**, 11828-11829.
13. M. Higashi, K. Domen and R. Abe, *J. Am. Chem. Soc.*, 2012, **134**, 6968-6971.
14. H. Fujito, H. Kunioku, D. Kato, H. Suzuki, M. Higashi, H. Kageyama and R. Abe, *J. Am. Chem. Soc.*, 2016, **138**, 2082-2085.
15. H. Kunioku, M. Higashi, O. Tomita, M. Yabuuchi, D. Kato, H. Fujito, H. Kageyama and R. Abe, *J. Mater. Chem. A*, 2018, **6**, 3100-3107.
16. D. Kato, K. Hongo, R. Maezono, M. Higashi, H. Kunioku, M. Yabuuchi, H. Suzuki, H. Okajima, C. Zhong, K. Nakano, R. Abe and H. Kageyama, *J. Am. Chem. Soc.*, 2017, **139**, 18725-18731.
17. A. Kudo, *J. Catal.*, 1988, **111**, 296-301.
18. S. Ikeda, M. Hara, J. N. Kondo, K. Domen, H. Takahashi, T. Okubo and M. Kakihana, *Chem. Mater.*, 1998, **10**, 72-77.
19. H. Kato, K. Asakura and A. Kudo, *J. Am. Chem. Soc.*, 2003, **125**, 3082-3089.
20. K. Maeda, K. Teramura, T. Takata, M. Hara, N. Saito, K. Toda, Y. Inoue, H. Kobayashi and K. Domen, *J. Phys. Chem. B*, 2005, **109**, 20504-20510.
21. K. Maeda and K. Domen, *J. Phys. Chem. C*, 2007, **111**, 7851-7861.
22. K. Maeda, N. Saito, Y. Inoue and K. Domen, *Chem. Mater.*, 2007, **19**, 4092-4097.
23. K. Maeda, H. Terashima, K. Kase, M. Higashi, M. Tabata and K. Domen, *Bull. Chem. Soc. Jpn.*, 2008, **81**, 927-937.
24. H. Kato and A. Kudo, *J. Phys. Chem. B*, 2001, **105**, 4285-4292.
25. A. M. Kusainova, S. Y. Stefanovich, V. A. Dolgikh, A. V. Mosunov, C. H. Hervoches and P. Lightfoot, *J. Mater. Chem.*, 2001, **11**, 1141-1145.
26. A. M. Kusainova, W. Zhou, J. T. S. Irvine and P. Lightfoot, *J. Solid State Chem.*, 2002, **166**, 148-157.
27. V. Petříček, M. Dušek and L. Palatinus, *Z. Kristallogr. Cryst. Mater.*, 2014, **229**, 345-352.
28. M. Sadakane, K. Sasaki, H. Kunioku, B. Ohtani, R. Abe and W. Ueda, *J. Mater. Chem.*, 2010, **20**, 1811.
29. N. Murakami, O. O. P. Mahaney, R. Abe, T. Torimoto and B. Ohtani, *J. Phys. Chem. C*, 2007, **111**, 11927-11935.
30. O.-O. Prieto-Mahaney, N. Murakami, R. Abe and B. Ohtani, *Chem. Lett.*, 2009, **38**, 238-239.
31. K. Maeda, N. Murakami and T. Ohno, *J. Phys. Chem. C*, 2014, **118**, 9093-9100.
32. F. Amano, M. Nakata, A. Yamamoto and T. Tanaka, *J. Phys. Chem. C*, 2016, **120**, 6467-6474.

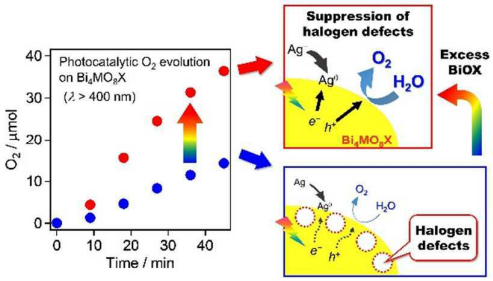

Preparation of Bi_4MO_8X with excess BiOX precursors substantially improved their photocatalytic activity for water oxidation by suppressing the formation of surface halogen defects.